ChemPubSoc Europe

DOI: 10.1002/chem.201702130

CHEMISTRY A European Journal Full Paper

Thin films

Decoding Nucleation and Growth of Zeolitic Imidazolate Framework Thin Films with Atomic Force Microscopy and Vibrational Spectroscopy

Zafer Öztürk, Matthias Filez, and Bert M. Weckhuysen*[a]

Abstract: The synthesis of metal-organic framework (MOF) thin films has garnered significant attention during the past decade. By better understanding the parameters governing the nucleation and growth of such thin films, their properties can be rationally tuned, empowering their application as (reactive) membranes. Here, a combined AFM-vibrational spectroscopy research strategy is employed to detail the chemistries governing the nucleation and growth of zeolitic imidazolate framework (ZIF) thin films, in particular isostructural Co-ZIF-67 and Zn-ZIF-8. First, a single step direct synthesis approach is used to investigate the influence of different synthesis parameters –metal/linker ratio, temperature, and metal type– on the thin film nucleation and growth behaviour. While the metal/linker ratio has a pronounced effect on the thin film nucleation rate, the temperature mainly influences the growth kinetics of nuclei forming the thin film. In addition, the nucleation and growth of ZIF thin films is shown to be highly dependent on the electronegativity of the metal type. Thin-film thickness control can be achieved by using a multistep synthesis strategy, implying repetitive applications of single step deposition under identical synthesis conditions, for which a growth mechanism is proposed. This study provides insight into the influence of synthesis parameters on the ZIF thin film properties, using tools at hand to rationally tune MOF thin film properties.

Introduction

Metal-organic frameworks (MOFs) are microporous crystalline materials built-up from metal oxide clusters interconnected by organic linkers.[1–8] By varying the metal and linker type, the MOF functionalities and pore space can be rationally tuned towards their desired properties.[5,9–12] This compositional flexibility makes MOFs extremely versatile functional materials, allowing their application in various fields,[13–15] including gas sensing,[10] separation,[6,10,16–18] storage,[19,20] and (photo-) catalysis.[18,21–25] Zeolitic imidazolate frameworks (ZIFs) are a sub-class of MOFs in which divalent metal cations, for example, Co^{2+}, Zn^{2+}, Cu^{2+}, or Fe^{2+}, are tetrahedrally coordinated by bridging imidazolate-type linkers.[26–31] In ZIFs, the resulting framework has a similar coordination geometry to those of microporous crystalline aluminosilicates, namely zeolites.[26,32–34] Owing to their resemblance to both zeolites and traditional MOFs, ZIFs combine the structural flexibility of MOFs with the thermal and chemical stability of zeolites,[26,29] as recently demonstrated in the fields of gas storage,[35–37] sensing,[38] and catalysis.[23,39,40] Amongst them, Zn-ZIF-8 is a quintessential model system of the ZIF family, being constructed through Zn^{2+} ions tetrahedrally coordinated by bridging 2-methylimidazolate linkers.[26,28,30,41–43] By using Co^{2+} instead of Zn^{2+} cations, isostructural Co-ZIF-67 is obtained, with an identical structure to Zn-ZIF-8 but with Co^{2+} in the Zn^{2+} lattice positions.[44–47]

Several studies report on the crystallisation mechanisms of bulk ZIFs by using in situ static light scattering (SLS),[29] transmission electron microscopy (TEM),[32,48] scanning electron microscopy (SEM),[28,49] X-ray diffraction (XRD),[28,32] small angle and wide angle X-ray scattering (SAXS/WAXS),[31] electrospray ionisation mass spectrometry (ESI-MS),[50] and atomic force microscopy (AFM).[51,52] However, for (reactive) membrane and gas sensor applications, conformal ZIF thin films with highly controllable morphologies are required instead of bulk powders. Two thin film deposition methods in particular have received much attention in the past years; layer-by-layer synthesis and direct solvothermal synthesis. Layer-by-layer synthesis relies on the alternating exposure of metal and linker solutions to a self-assembled monolayer (SAM)-terminated substrate. This method provides high thickness and orientational control, but is slow and economically not viable, except for specialty applications. In contrast, direct synthesis combines the metal and linker solutions in a single mixed solution, and offers rapid thin film growth at the expense of morphological con-

[a] Z. Öztürk, Dr. M. Filez, Prof. Dr. B. M. Weckhuysen
Inorganic Chemistry and Catalysis
Debye Institute for Nanomaterials Science
Utrecht University
Universiteitsweg 99, 3584 CG Utrecht (The Netherlands)
E-mail: b.m.weckhuysen@uu.nl

Supporting information for this article and ORCID(s) for the author(s) can be found under:
https://doi.org/10.1002/chem.201702130.

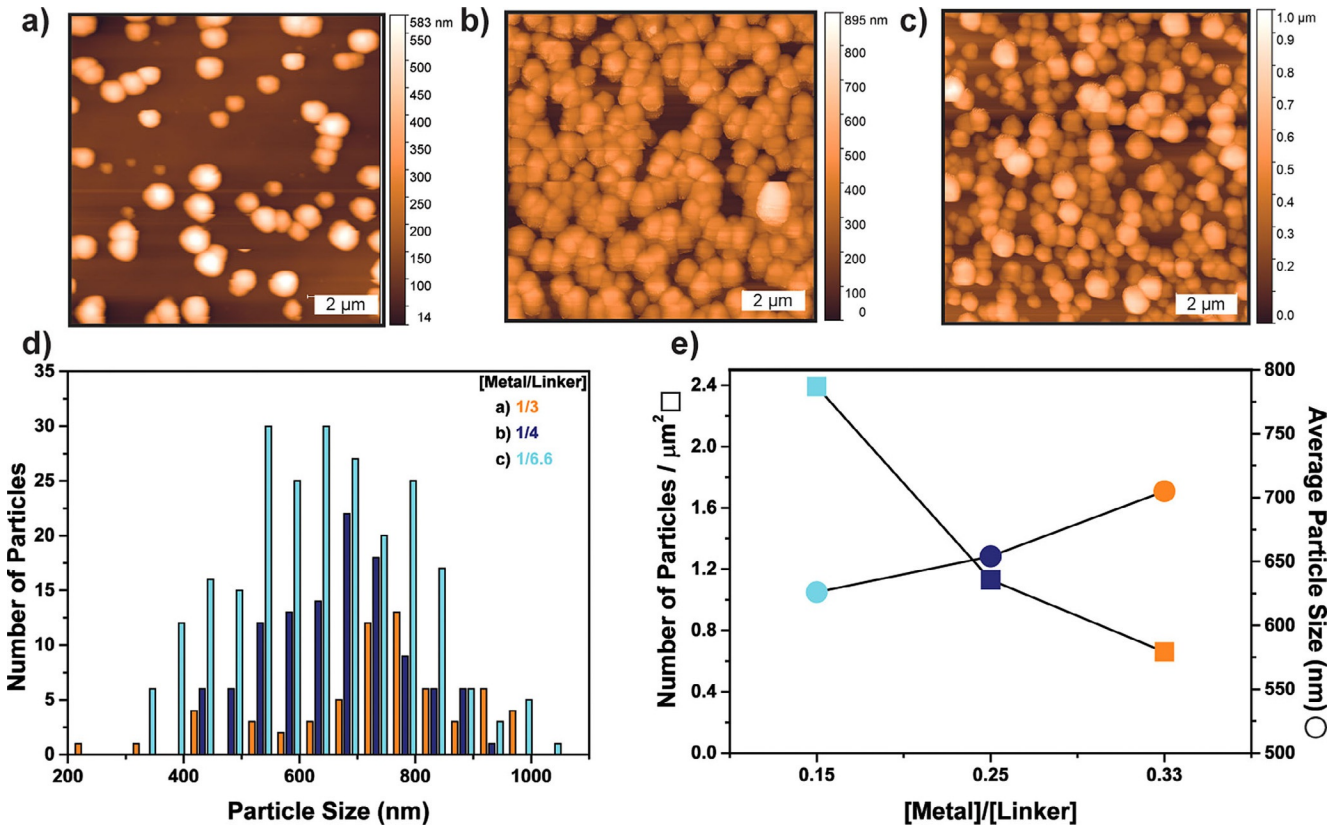

Figure 1. AFM micrographs for the Co-ZIF-67 thin films prepared at different metal to linker concentrations a) 1/3, b) 1/4, c) 1/6.6. The resulting particle size histograms d), and e) the variation of number of particles per μm^2 and average particle size at the aforementioned concentration regime.

trol.[4,8,11,53] However, fundamental improvement of the morphology of directly synthesised thin film is still possible. This could potentially allow this industrially viable method to tailor thin film properties at a comparable level relative to layer-by-layer grown films. Strong improvements, however, rely on the advent and application of advanced characterisation tools, which can fill the knowledge gap to achieve such thin film design.

The nucleation and growth behaviour of ZIF thin films, to the best of our knowledge, has not been studied before, and in particular the role of synthesis parameters has not been reported in a systematic way. Here, a combined AFM-vibrational spectroscopy research strategy is presented to investigate the chemistries governing the nucleation and growth of ZIF thin films. In particular, single step deposition through the direct synthesis method is utilised for the investigation of different synthesis parameters; namely metal/linker ratio, temperature, and metal type. In addition, a multistep direct synthesis method is further employed for controlling the thickness of Co-ZIF-67 and Zn-ZIF-8 thin films. Finally, a mechanism regarding the multistep thin film growth mechanism is proposed.

Results and Discussion

Single step deposition

Three sets of experiments were carried out to study the impact of the 1) metal/linker ratio, 2) synthesis temperature, and 3) metal cation on the nucleation and growth behaviour of Co-ZIF-67 thin films prepared in MeOH. First, the influence of the metal/linker ratio on the resulting ZIF particle deposition –being the onset of thin film formation– is studied by atomic force microscopy (AFM). Figure 1 a–c, respectively shows three AFM topology maps (10×10 μm) of Co-ZIF-67 particles deposited on an Au coated substrate after 10 min at room temperature with metal/linker ratios of 1:3, 1:4, and 1:6.6 (see Experimental Section). Visual inspection of the AFM micrographs clearly shows that the number of particles increases with decreasing metal/linker ratio. In order to quantify this observation, particle size histograms are obtained, as shown in Figure 1 d. Based on these histograms, the number of particles increases in an order of 66, 113, and 239 per 100 μm^2 with decreasing metal/linker ratio from 1:3 to 1:6.6 (Figure 1 e), respectively. In addition, the particle size histograms show a significant average particle size increase with increasing metal/linker ratio within the investigated range. These results imply that the number of nuclei increases with increasing linker concentration, at the expense of the eventual nucleus size, which decreases. Furthermore, the particle histograms in Figure 1 d show congruent shapes –within experimental errors– across different metal/linker conditions. It is clear that for all metal/linker cases small particles are always observed in the presence of larger ones (Figure 1a–d), suggesting that nucleation of new nuclei is a frequent and an ongoing process throughout the 10 min synthesis time. Complementary characterisation by Raman spectroscopy and X-ray diffraction (XRD) is performed

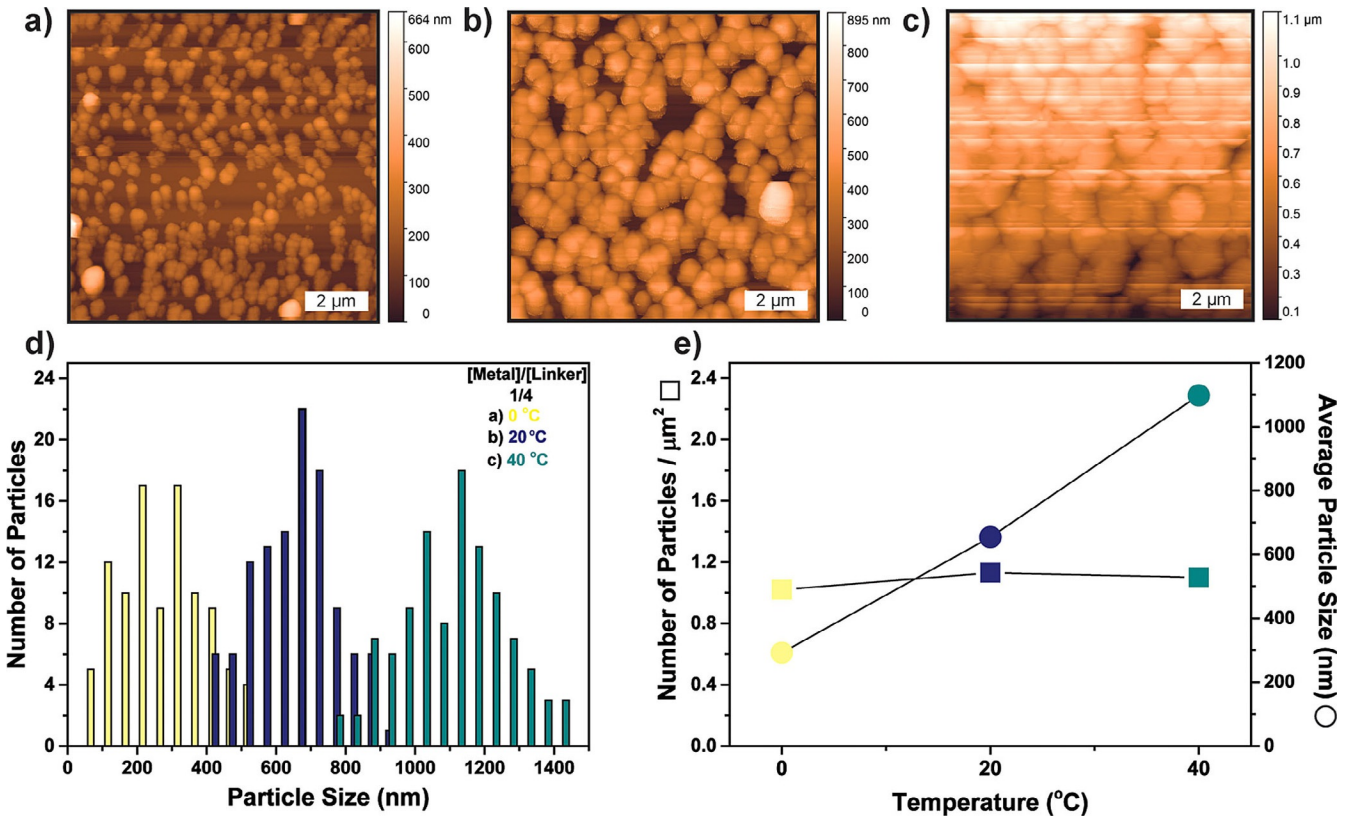

Figure 2. AFM micrographs of Co-ZIF-67 thin films prepared at a) 0 °C, b) 20 °C, c) 40 °C. The resulting particle size histograms d), and e) the variation of number of particles per μm^2 and average particle size at the aforementioned temperature regime.

for all samples and shown in Supporting Information Figures S1–S4, respectively.

In the second set of experiments, the effect of the synthesis temperature was examined by performing deposition at 0, 20, and 40 °C, while keeping the metal to linker ratio (1:4) and reaction time (10 min) constant. The resulting Co-ZIF-67 thin films on a gold-coated substrate were probed by AFM (10× 10 µm) as illustrated in Figure 2 a–c. Visual inspection of the AFM micrographs demonstrates that the average particle sizes increase with increasing synthesis temperature, while the number of nuclei remains constant. Indeed, the quantified AFM histograms (Figure 2 d–e) show that the overall number of particles detected is constant within experimental error, but that the average particle size significantly increases upon temperature increase. More precisely, the average calculated particle sizes range from 292 to 654, and 1098 nm for temperatures from 0, 20, and 40 °C, respectively (Figure 2 e). Such temperature-induced particle growth clearly results in an increase in the surface coverage. These results point out that nucleus size increases with an increase in the temperature, whereas the number of nuclei formed is not affected in a lesser amount within the temperature range under study.

Figure 3 a illustrates a proposed reaction Scheme, which leads to the formation of Zn-ZIF-8 and Co-ZIF-67. The mechanism involves three reaction steps: 1) linker coordination of Co^{2+} centres, 2) deprotonation of the 2-methylimidazole linker(s), and 3) oligomerisation by linking together different Co^{2+} centres through deprotonated 2-methylimidazole ligands. The effect of varying metal/linker ratio and temperature can be explained by taking into account the proposed reaction mechanism. The increase in the linker concentration (decreasing metal/linker ratio) gives rise to an increase in the rate and extent of ligand exchange reactions between 2-methylimidazole linkers and methanol/water/nitrate ligands around Co^{2+}. Hence a higher linker concentration will lead to a Co^{2+} coordination sphere, which is more abundant in 2-methylimidazole linkers, established in a shorter period of time. As a result, a higher concentration of linker coordinated Co^{2+} complexes will result in an increased reaction rate of 2-methylimidazole deprotonation. These deprotonated Co^{2+} complexes are vital for nucleation, since a single deprotonated 2-methylimidazole ligand can bridge two Co^{2+} centres, leading to oligomerisation and therefore nucleus formation. It is thus expected that the nucleation rate increases for higher linker concentrations owing to the increase in the deprotonation rate, eventually yielding more nuclei/particles for higher linker concentrations (i.e., lower metal/linker ratios). Apparently, more nuclei formed per μm^2 leads to smaller particles, as shown in the AFM micrographs (Figure 1). This can be rationalised by the fact that metal and linker constituents in the solution are to be distributed amongst a larger number of nuclei for lower metal/linker ratios, leading to smaller particles. These findings regarding the eventual nucleus size are in harmony with previously re-

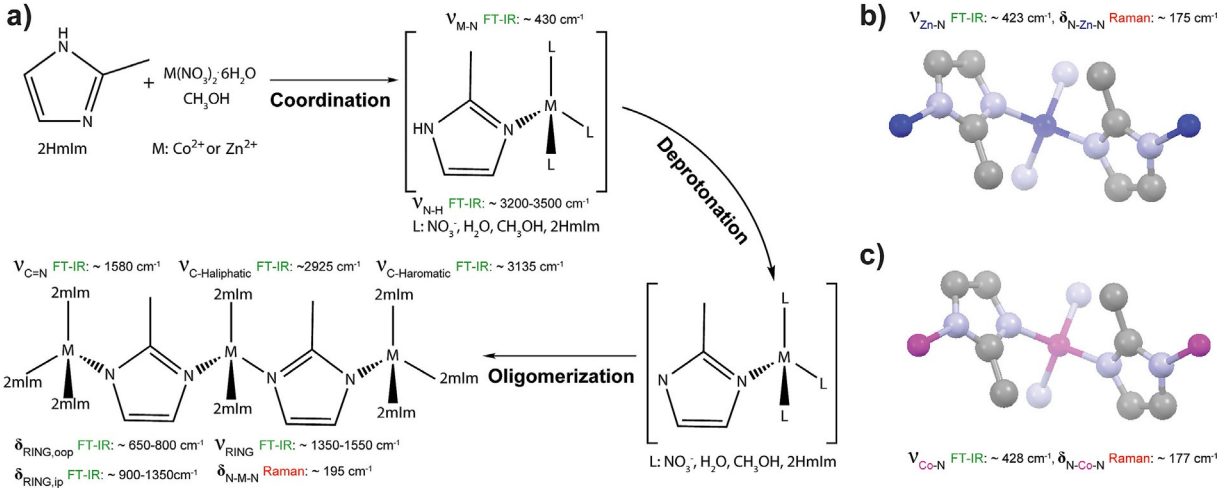

Figure 3. a) Proposed mechanism for the formation of Zn-ZIF-8 and its cobalt variant Co-ZIF-67 along with the characteristic FTIR and Raman band signatures, b) coordination sphere of Zn-ZIF-8, and c) coordination sphere of Co-ZIF-67 (hydrogen atoms are omitted for clarity, grey: carbon, light blue: nitrogen, dark blue: zinc, purple: cobalt).

ported literature results of Cravillon et al., Lim et al., and Saha et al.[29,50,54]

The influence of the synthesis temperature is significantly different compared to the metal/linker ratio. For increasing temperatures, the number of nuclei remains constant, but their eventual size increases significantly after 10 min of synthesis time. This suggests that the nucleation rate is not affected by a temperature change, though the growth rate is strongly sensitive to temperature alterations. Alternatively, it could be hypothesised that the oligomerisation rate exhibits a strong temperature dependency. By increasing the temperature, the activation energy of oligomerisation can be overcome more easily, eventually yielding larger particles. While the linker/metal ratio has a major influence on the nucleation rate –though the particle size is also influenced– the temperature only influences the eventual size of the particles deposited in the thin film. This knowledge uses tools at hand to rationally tune the size of particles by changing the synthesis temperature.

For the third set of experiments, the influence of the metal ion type on the nucleation and growth is examined by comparing isostructural Co-ZIF-67 and Zn-ZIF-8 under identical synthesis conditions (metal/linker = 1:4, room temperature, and 10 min deposition time). AFM micrographs, along with the corresponding particle size distributions of Zn-ZIF-8 and Co-ZIF-67 thin films, are shown in Figure 4a. The average particle sizes were calculated as 75 and 626 nm for Zn-ZIF-8 and Co-ZIF-67, respectively. However, the number of nuclei formed for single layered Zn-ZIF-8 was observed to be doubled, compared to the number of particles nucleated for single layered Co-ZIF-67 (Figure 4a). It can be seen that the surface area below the curve for Co-ZIF-67 is much larger compared to Zn-ZIF-8. This implies that the total amount of material deposited for Co-ZIF-67 is exceedingly large compared to the Zn-ZIF-8 case, suggesting more rapid growth for Co-ZIF-67. This particle size analysis shows that Co-ZIF-67 nucleates and grows faster under the same synthesis conditions, which will be explained in more detail below.

Multistep deposition

As shown above, the particle size and density in ZIF thin films can be controlled by the synthesis temperature and linker/metal ratio. Obtaining fully closed films initially, and tuning the ZIF thin films thickness in a later stage of deposition, is another film parameter to be controlled. This can be achieved by multilayer growth, implying repetitive layer deposition. In order to assess the controllability of this synthetic strategy, a combined AFM-vibrational spectroscopy investigation is performed for thin films obtained through one, two, and four deposition steps. Figure 4 shows the AFM data of Zn-ZIF-8 and Co-ZIF-67 thin films deposited by two (Figure 4b) and four (Figure 4c) deposition steps besides single step deposition previously discussed (Figure 4a). First, the AFM micrographs show a coverage increase of the Au substrate with increasing number of deposition cycles for both Zn-ZIF-8 and Co-ZIF-67 thin films. The particles on the top surface of the thin film display a clear Gaussian distribution, from which the average and standard deviation are plotted in graphs of Figure 4d–e, respectively. The average particle size of Co- and Zn-based thin films increases to a similar absolute extent as a result of film closure and growth. Likewise, a significant broadening is observed in the particle size distribution for both film types, as evident from the Gaussian standard deviation. This broadening is a consequence of the growth mechanism schematically represented in Figure 5. During the first deposition step, ZIF particles are nucleated on the Au substrate surface and/or deposited from the synthesis solution. During the next step, these particles gradually grow through assembly from (oligomerised) linker-coordinated metals in the synthesis solution. In addition, newly nucleated particles are deposited on top of the particle layer, grown during step 1. After multiple steps, the particle

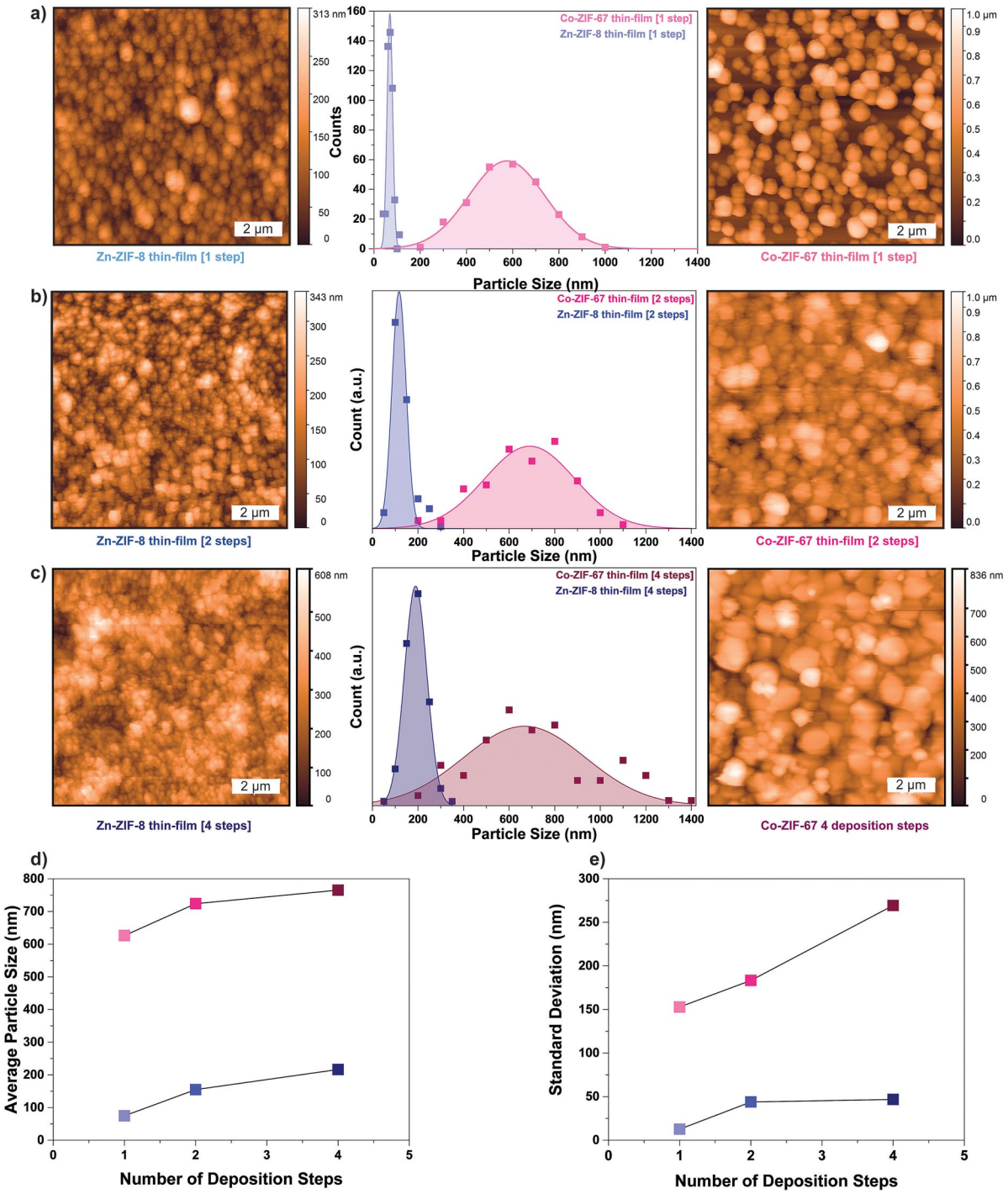

Figure 4. Comparison of AFM micrographs and particle size distributions of Zn-ZIF-8 and Co-ZIF-67 thin films obtained through a) 1 step deposition, b) 2 steps deposition, and c) 4 steps deposition. The variation of number of particles per μm^2 and average particle size through multiple deposition steps d), and e) standard deviation of the given particle size distributions (Metal/linker: 1:6.6, 20 °C, each deposition step with a time of 10 min).

layer becomes an increasingly intergrown thin film through growth from the synthesis solution, yielding a polycrystalline intergrown ZIF thin film. Indeed, SEM confirms the presence of a closed film on which newly nucleated, rhombic dodecahedrally shaped ZIF particles are deposited during the last synthesis step of the multistep process (Figure 5). This growth mechanism is compatible with the particle broadness observation in the AFM histograms, which arises from 1) previously deposited particles which increased size through repetitive growth from the synthesis solution, in combination with 2) newly deposited (smaller) ZIF particles at the top surface. These findings suggest that, through the proposed multiple deposition step approach, eventual particle size and density, as well as surface coverage/film thickness, can be manipulated. This can be achieved by selecting the correct synthesis conditions, including the optimal 1) metal/linker ratio, 2) tempera-

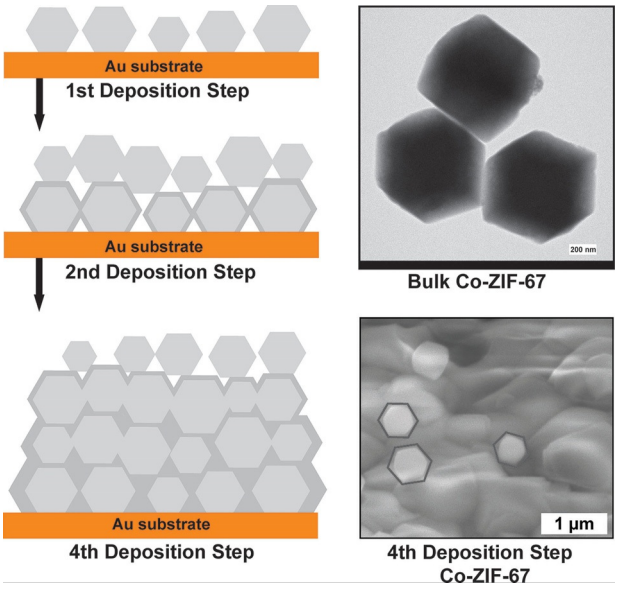

Figure 5. (left) Mechanism proposed regarding ZIF thin film growth through direct synthesis method with multiple deposition steps; (right, top) TEM of bulk Co-ZIF-67 crystals shown in schematic representation; (right, bottom) SEM image of Co-ZIF-67 thin film after 4 deposition steps.

ture, and 3) the number of deposition steps. The thickness of thin films can also be varied by a method proposed by Caro et al.[55] However the multi-step approach proposed here can achieve better control over thickness of the film in particular, as well as a control over the other aforementioned film properties (grain size and density of particles).

Besides AFM mapping of the Co- and Zn-based thin film morphology, complementary chemical information is gained by vibrational spectroscopy, namely diffuse reflectance infrared Fourier-transformed spectroscopy (DRIFTS) and Raman spectroscopy. DRIFT spectroscopy measurements are carried out in a spectral region ranging from 400–4000 cm^{-1} in order to provide molecular scale chemical bond information. Figure 6a displays the DRIFTS spectra of the Zn-ZIF-8 and Co-ZIF-67 thin films obtained after 4 depositions steps, as well as their bulk analogues and the 2-methylimidazole linker references. DRIFTS spectra of the thin films of Zn-ZIF-8 and Co-ZIF-67 obtained after 1 and 2 step depositions are provided in Figure S5 (Supporting Information), displaying similar spectral features compared to their 4 step analogues.

In general, the Zn-ZIF-8 and Co-ZIF-67 thin film spectra obtained after four deposition steps exhibit IR bands which are typical of bulk ZIF materials.[41,56–59] In particular, going from low to high wavenumbers, multiple bending/stretching vibrations are identified: Co–N/Zn–N stretching (≈430 cm^{-1}), ring out-of-plane bending (≈650–800 cm^{-1}), ring in-plane bending (≈900–1350 cm^{-1}), ring stretching (≈1350–1550 cm^{-1}), C=N stretching (≈1580 cm^{-1}), CH_3 (≈2925 cm^{-1}), and C–H aromatic (≈3135 cm^{-1}) stretching modes. In Figure 3a–c and Figure 6a, characteristic vibrations are highlighted as observed for both Zn-ZIF-8 and Co-ZIF-67 (thin films).[41,45,56,57,59] A detailed comparison between the IR spectra of bulk and thin film grown materials shows that more distinct IR bands are observable for bulk ZIFs, especially in the ring stretching and vibrational regions (≈830, 940, 1070, 1240 cm^{-1}, etc.).This suggests that bulk ZIF framework is less defective/perturbed in nature relative to its thin film analogue, leading to less bond/ring disorder. Note that the absence of broad N–H stretching bands in the region between 3200–3500 cm^{-1} in the DRIFT spectra of Zn-ZIF-8 and Co-ZIF-67 demonstrate that the linker 2-methylimidazole is incorporated in the ZIF-8/-67 thin films in its deprotonated state.[60] A detailed look into the Co–N and Zn–N stretching region (Figure 6b) of Co-ZIF-67 and Zn-ZIF-8 thin film IR spectra shows a blue shift for Co- (≈428 cm^{-1}) relative to Zn-based (≈423 cm^{-1}) thin films. The more electronegative nature of Co^{2+} compared to Zn^{2+} induces more ionised bonds,[45] leading to more tight bonds with M–N stretching vibrations at higher wavenumbers. The spectral shift observed for the metal–nitrogen vibrations is supported by DFT calculations reported by Krokidas et al. The authors obtained a higher force constant for Co-ZIF-67 compared to Zn-ZIF-8.[61] Furthermore, Krokidas et al. simulated the Zn–N/Co–N bond length and angle, yielding 1.98 Å Zn–N and 1.96 Å Co–N bond lengths, in line with stronger Co–N bonds.

The more electronegative nature of Co^{2+} is not only manifested at the molecular scale. Its higher reactivity/electronega-

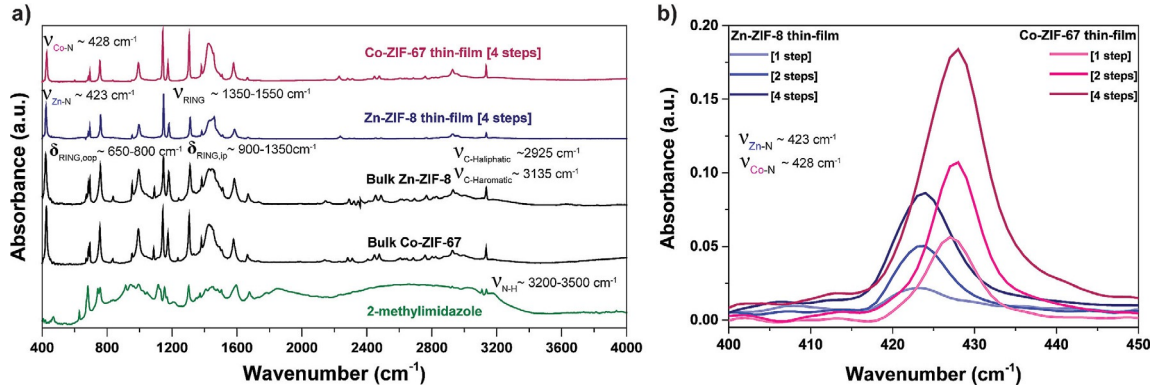

Figure 6. a) Comparison of DRIFT spectra of the 2-methylimidazole linker, bulk Co-ZIF-67, bulk Zn-ZIF-8, Zn-ZIF-8, and Co-ZIF-67 thin films obtained by 4 deposition steps, b) DRIFT spectra in the region of 400–450 cm^{-1} for Zn-ZIF-8 and Co-ZIF-67 thin films obtained through 1, 2, and 4 deposition steps. The characteristic bands were also provided.

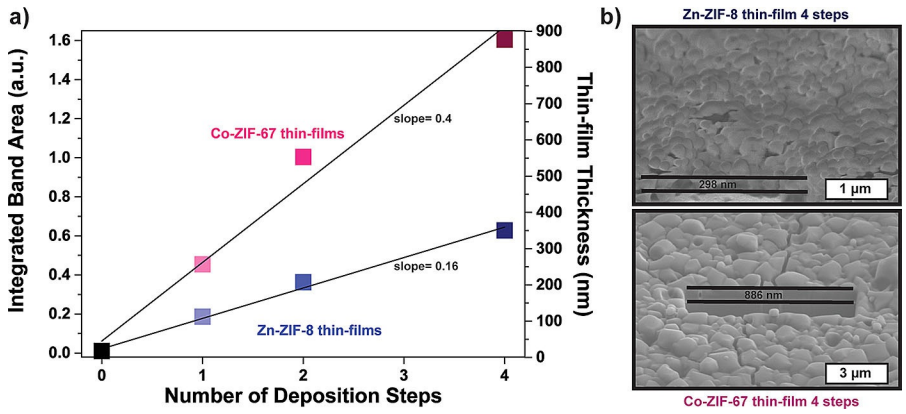

Figure 7. a) The variation of absorbance in terms of integrated band area and expected thin film thickness as a function of number of deposition steps, b) FIB-SEM image and the cross-section thickness of the Zn-ZIF-8 and Co-ZIF-67 thin films prepared with 4 deposition steps.

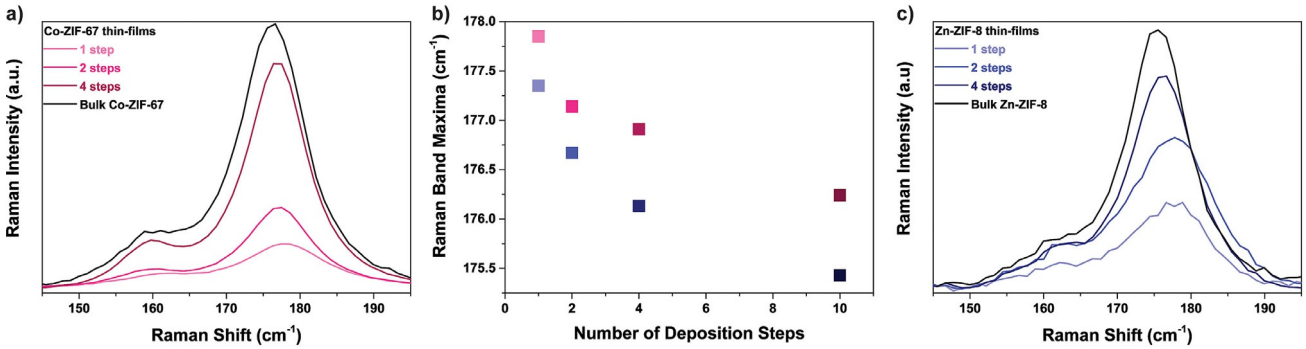

Figure 8. Comparison of Raman spectra of a) Co-ZIF-67 thin films obtained after 1, 2 and 4 deposition steps along with bulk Co-ZIF-67, c) Zn-ZIF-8 thin films obtained after 1, 2 and 4 deposition steps along with their bulk analogue in the region of 145–195 cm^{-1}. b) Raman band maxima (deformation mode, N-M-N) vs. number of deposition steps for the bands shown in a) and c).

tivity results in a faster nucleation and growth, as microscopically observed by AFM. Therefore, the chemically sensitive information abstracted by IR can, in strong connection with AFM, provide the underlying clarification for film properties manifested at a microscopic level.

Further linking of IR information to the Zn-ZIF-8 and Co-ZIF-67 thin film morphology can be achieved by using the Co-N/Zn-N vibrational band intensities as markers for the thickness of Zn-ZIF-8 and Co-ZIF-67 thin films. Indeed, AFM allows imaging of the top surface of thin films, and is therefore ideal to study the onset of thin film nucleation and growth, but cannot provide thickness information after film closure. In this respect, IR can probe bulk information in contrast to surface sensitive AFM. In Figure 6b, an intensity increase of the Zn–N and Co–N spectral bands is observed upon deposition of multiple steps. In Figure 7a, the integrated areas below these bands are plotted versus the number of deposition steps: the band areas are proportional to the average film thickness. The latter is calibrated through measurement of the local thickness of Zn-ZIF-8 (≈300 nm) and Co-ZIF-67 (≈900 nm) thin films after four deposition steps by focused ion beam SEM (FIB-SEM, Figure 7b). These trends confirm that the nucleation and growth rate of Co-ZIF-67 thin films exceeds the one of Zn-ZIF-8. In addition, a linear increase in the film thickness is observed within experimental uncertainty for both Co-ZIF-67 and Zn-ZIF-8 thin films synthesised by multistep synthesis. This is a natural consequence of the fact that during the multistep synthesis method, every step involves an identical direct synthesis solution, which is contacted with the thin film under the same reaction time. This repetitive synthetic protocol is therefore ideally suited for the thickness control of ZIF thin films on the micrometre scale. The as-prepared thin films were further characterised by Raman spectroscopy and XRD (see Supporting Information Figure S6 and S7).

Finally, Raman spectroscopy measurements are performed for Zn-ZIF-8 and Co-ZIF-67 thin films along with their bulk analogues. Figure 8a and b illustrate the comparison of Zn-ZIF-8 and Co-ZIF-67 thin films in the region of 145–195 cm^{-1} where the nitrogen-metal-nitrogen (N-M-N) deformation vibration is observed (Figure 3).[62] Figure 8b shows the variation in the N-M-N band maxima with one, two, and four deposition steps. This characteristic band is located at higher wavenumbers for Co-ZIF-67 than that of Zn-ZIF-8 for all deposition steps (including bulk analogues).

The differing spectral positions of the Zn-ZIF-8 and Co-ZIF-67 series observed for the N-M-N vibration is in line with the DRIFTS data, showing the presence of more stiff N-Co-N bonds compared to N-Zn-N, which can be attributed to the higher

electronegativity/ionicity of cobalt bonds. In addition, the band maxima slightly shifts from higher to lower wavenumber with increasing deposition steps indicating that the force constant decreases for both Zn-ZIF-8 and Co-ZIF-67 thin films. It is plausible to propose that the more intergrown films undergo a bond relaxation to a certain extent owing to an increased structural stability.

Conclusion

The influence of different synthesis parameters on the formation and properties of isostructural Co-ZIF-67 and Zn-ZIF-8 thin films is investigated. Direct synthesis is employed for ZIF thin film deposition; a method involving both metal and linker constituents in a single solution.

To unravel the influence of synthesis parameters, such as 1) metal/linker ratio, 2) temperature, and 3) metal type, a single deposition step is used. Atomic force microscopy (AFM) is utilised to map the surface topology in 10×10 μm regions at the initial stages of ZIF thin film formation, allowing quantification of the number and size of deposited ZIF nuclei during synthesis. A decreasing metal/linker ratio –that is, higher linker concentration– induces a higher nucleation rate, resulting in an increased number of nuclei populating the early thin film structure. It is suggested that the nucleus size is inversely proportional to the number of nuclei when varying the metal/linker ratio. A factor strongly dictating the particle size is the synthesis temperature: while the number of nuclei remains constant, the particle size strongly increases with increasing thermal activation. Finally, Co as the constituent metal in Co-ZIF-67 exhibits more reactive nucleation and growth behaviour compared to Zn in isostructural Zn-ZIF-8. This is caused by the higher electronegativity of Co^{2+} cations compared to Zn^{2+}, leading to more polarised/ionic Co–N bonds relative to Zn–N. This has been clearly observed in the Co/Zn-N stretching vibration in infrared (IR) spectroscopy, where the Co–N vibrational band is blue shifted by 5 cm^{-1} relative to the Zn–N vibrational band.

While the number and size of particles constituting the thin film can be controlled by parameters, such as metal/linker ratio and the temperature, the eventual film thickness can be tuned by multistep direct synthesis. By repetitive single step synthesis, a linear growth rate is observed by bulk IR with the number of repeating synthesis steps. During the first deposition step, new nuclei populate the substrate surface. After multiple steps, however, pre-existing particles undergo continuous growth and coalesce, leading to film closure. In addition, newly nucleated particles are deposited on top of the film. In general, it is observed for all ZIF thin films that the IR spectra contain less pronounced features compared to bulk ZIF-67 and ZIF-8. This suggests that the thin film structure, at the molecular level, is more perturbed, that is, more defective in nature.

Finally, this work shows that coupling molecular-scale vibrational spectroscopy information with topologic knowledge acquired through atomic force microscopy aids in linking molecular interactions, which manifest at the microscale of the thin film morphology. As a future prospect, the investigation of the reaction time can give further insights into the nucleation and growth processes of ZIF thin films.

Experimental Section

Bulk Zn-ZIF-8 and Co-ZIF-67 synthesis

The synthesis of bulk Zn-ZIF-8 and Co-ZIF-67 have been reported previously and we have used these literature recipes.[29, 32] In a typical synthesis, 0.3 g of $Zn(NO_3)_2{\cdot}6H_2O$ (Sigma–Aldrich, 99%) and 0.66 g of 2-methylimidazole (Sigma–Aldrich, 99%) were dissolved separately in 11.3 g of methanol (Acros, extra dry). The organic linker solution was transferred into the Zn-based solution and the corresponding mixture was stirred and let to react for 24 h. The solid ZIF-8 particles were collected from solution by centrifugation at 4000 rpm for 10 min and washed with methanol. After washing with methanol, the solution was centrifuged again and washed with methanol. The ZIF-8 material was dried at room temperature for 24 h and then further dried in an oven at 75 °C overnight. For the synthesis of Co-ZIF-67, $Co(NO_3)_2{\cdot}6H_2O$ (Acros, 99%) was used as a precursor and the same procedure was followed as for the synthesis of Zn-ZIF-8.

Co-ZIF-67 and Zn-ZIF-8 thin film synthesis

The room temperature preparation of Zn-ZIF-8 and Co-ZIF-67 thin films through the direct synthesis method was described previously by Tu et al.[3] and adapted for this work. For the preparation of thin films with metal/linker ratio of 1:4 of Co-ZIF-67, a methanolic (Acros, extra dry) solution of 40 mM $Co(NO_3)_2{\cdot}6H_2O$ (Sigma–Aldrich, 99%) and a methanolic (Acros, extra dry) solution of 160 mM 2-methylimidazole (Sigma–Aldrich, 99%) were used. Within all sets of experiments, the metal concentration was kept constant, and the linker concentration in the solution was varied to obtain different metal/linker ratios. During the experiments, 1:3, 1:4, and 1:6.6 metal/linker ratios were used. Gold-coated silicon wafers (60 nm Au particles sputtered on silicon wafer with a Ge adhesion layer) were used as substrates and were purchased from AMOLF (The Netherlands). 4 mL of both metal and linker solutions were mixed in a glass vial and the substrate was immersed for 10 min vertically into the solution in order to avoid sedimentation. This process is called the deposition step. One, two, and four deposition steps were applied in this work, where the intermediate washing steps with fresh methanol have been followed by a gentle drying by flowing N_2. For the preparation of Zn-ZIF-8 thin films, the same procedure was performed where $Zn(NO_3)_2{\cdot}6H_2O$ (Acros, 99%) was used as the metal precursor. Finally, an ice-bath and water-bath were used for maintaining 0 °C and 40 °C, respectively with a strict temperature control.

Characterisation

Atomic force microscopy (AFM) measurements were performed on a NT-MDT NTEGRA Spectra upright AFM unit. Olympus AC 160TS tips were used for all AFM measurements. AFM scans of 10×10 μm in size were made with high resolution (i.e., 512×512 pt). The iTEM software was used for the particle size analysis performed on AFM micrographs. Focused Ion Beam Scanning Electron microscopy (FIB-SEM) measurements were carried out with a Helius 600 FEI instrument, with an acceleration voltage of 2 kV and working distance of 4 mm, by using secondary electrons. A gallium source is used for the focused ion beam (FIB) operating at 30 kV. Diffuse reflectance infrared Fourier transform (DRIFT) spectroscopy experi-

ments were carried out by using a Praying Mantis™ Diffuse Reflection Accessory (Harrick) in a PerkinElmer Frontier spectrometer equipped with DTGS detector. The spectra were collected over 64 scans in the region of 400–4000 cm^{-1} with a 4 cm^{-1} resolution. Raman spectroscopy measurements were performed with a Renishaw InVia micro-spectrometer making use of a 785 nm laser and the spectra were recorded in the spectral region of 100–3200 cm^{-1}.

Acknowledgements

M.F. acknowledges the European Horizon 2020 program Marie Skłodowska-Curie fellowship, while B.M.W. acknowledges the Dutch National Research School Combination Catalysis (NRSC-C), The Netherlands Organisation for Scientific Research (NWO) Gravitation program (Netherlands Center for Multiscale Catalytic Energy Conversion, MCEC) and the European Research Council (ERC) Advanced Grant (no. 321140).

Conflict of interest

The authors declare no conflict of interest.

Keywords: atomic force microscopy · nucleation · thin films · vibrational spectroscopy · zeolitic imidazolate frameworks

[1] G. Férey, *Chem. Soc. Rev.* **2008**, *37*, 191 – 214.
[2] M. Tu, S. Wannapaiboon, R. A. Fischer, *Dalton Trans.* **2013**, *42*, 16029 – 16035.
[3] M. Tu, S. Wannapaiboon, K. Khaletskaya, R. A. Fischer, *Adv. Funct. Mater.* **2015**, *25*, 4470 – 4479.
[4] O. Shekhah, J. Liu, R. A. Fischer, C. Wöll, *Chem. Soc. Rev.* **2011**, *40*, 1081 – 1106.
[5] S. T. Meek, J. A. Greathouse, M. D. Allendorf, *Adv. Mater.* **2011**, *23*, 249 – 267.
[6] S. Qiu, M. Xue, G. Zhu, *Chem. Soc. Rev.* **2014**, *43*, 6116 – 6140.
[7] D. J. Tranchemontagne, J. L. Mendoza-Cortés, M. O'Keeffe, O. M. Yaghi, *Chem. Soc. Rev.* **2009**, *38*, 1257 – 1283.
[8] A. Bétard, R. A. Fischer, *Chem. Rev.* **2012**, *112*, 1055 – 1083.
[9] O. M. Yaghi, M. O'Keeffe, N. W. Ockwig, H. K. Chae, M. Eddaoudi, J. Kim, *Nature* **2003**, *423*, 705 – 714.
[10] B. Liu, *J. Mater. Chem.* **2012**, *22*, 10094 – 10101.
[11] D. Zacher, O. Shekhah, C. Wöll, R. A. Fischer, *Chem. Soc. Rev.* **2009**, *38*, 1418.
[12] N. W. Ockwig, O. Delgado-Friedrichs, M. O'Keeffe, O. M. Yaghi, *Acc. Chem. Res.* **2005**, *38*, 176 – 182.
[13] A. U. Czaja, N. Trukhan, U. Müller, *Chem. Soc. Rev.* **2009**, *38*, 1284 – 1293.
[14] R. J. Kuppler, D. J. Timmons, Q.-R. Fang, J.-R. Li, T. A. Makal, M. D. Young, D. Yuan, D. Zhao, W. Zhuang, H.-C. Zhou, *Coord. Chem. Rev.* **2009**, *253*, 3042 – 3066.
[15] U. Mueller, M. Schubert, F. Teich, H. Puetter, K. Schierle-Arndt, J. Pastré, *J. Mater. Chem.* **2006**, *16*, 626 – 636.
[16] H. B. Tanh Jeazet, C. Staudt, C. Janiak, *Dalton Trans.* **2012**, *41*, 14003 – 14027.
[17] J.-R. Li, R. J. Kuppler, H.-C. Zhou, *Chem. Soc. Rev.* **2009**, *38*, 1477 – 1504.
[18] H.-L. Jiang, Q. Xu, *Chem. Commun.* **2011**, *47*, 3351 – 3370.
[19] A. C. McKinlay, B. Xiao, D. S. Wragg, P. S. Wheatley, I. L. Megson, R. E. Morris, *J. Am. Chem. Soc.* **2008**, *130*, 10440 – 10444.
[20] M. Eddaoudi, J. Kim, N. Rosi, D. Vodak, J. Wachter, M. O'Keeffe, O. M. Yaghi, *Science* **2002**, *295*, 469 – 472.
[21] M. Ranocchiari, J. A. van Bokhoven, *Phys. Chem. Chem. Phys.* **2011**, *13*, 6388 – 6396.
[22] J. Gascon, M. D. Hernández-Alonso, A. R. Almeida, G. P. M. van Klink, F. Kapteijn, G. Mul, *ChemSusChem* **2008**, *1*, 981 – 983.
[23] C. Chizallet, S. Lazare, D. Bazer-Bachi, F. Bonnier, V. Lecocq, E. Soyer, A.-A. Quoineaud, N. Bats, *J. Am. Chem. Soc.* **2010**, *132*, 12365 – 12377.
[24] E. V. Ramos-Fernandez, M. Garcia-Domingos, J. Juan-Alcañiz, J. Gascon, F. Kapteijn, *Appl. Catal. A* **2011**, *391*, 261 – 267.
[25] J. Gascon, A. Corma, F. Kapteijn, F. X. Llabrés i Xamena, *ACS Catal.* **2014**, *4*, 361 – 378.
[26] K. S. Park, Z. Ni, A. P. Cote, J. Y. Choi, R. Huang, F. J. Uribe-Romo, H. K. Chae, M. O'Keeffe, O. M. Yaghi, *Proc. Natl. Acad. Sci. USA* **2006**, *103*, 10186 – 10191.
[27] Z. Öztürk, J. P. Hofmann, M. Lutz, M. Mazaj, N. Z. Logar, B. M. Weckhuysen, *Eur. J. Inorg. Chem.* **2015**, *2015*, 1625 – 1630.
[28] J. Cravillon, C. A. Schröder, H. Bux, A. Rothkirch, J. Caro, M. Wiebcke, *CrystEngComm* **2012**, *14*, 492 – 498.
[29] J. Cravillon, R. Nayuk, S. Springer, A. Feldhoff, K. Huber, M. Wiebcke, *Chem. Mater.* **2011**, *23*, 2130 – 2141.
[30] J. Cravillon, S. Münzer, S.-J. Lohmeier, A. Feldhoff, K. Huber, M. Wiebcke, *Chem. Mater.* **2009**, *21*, 1410 – 1412.
[31] J. Cravillon, C. A. Schröder, R. Nayuk, J. Gummel, K. Huber, M. Wiebcke, *Angew. Chem. Int. Ed.* **2011**, *50*, 8067 – 8071; *Angew. Chem.* **2011**, *123*, 8217 – 8221.
[32] S. R. Venna, J. B. Jasinski, M. A. Carreon, *J. Am. Chem. Soc.* **2010**, *132*, 18030 – 18033.
[33] A. Phan, C. J. Doonan, F. J. Uribe-Romo, C. B. Knobler, M. O'Keeffe, O. M. Yaghi, *Acc. Chem. Res.* **2010**, *43*, 58 – 67.
[34] H. Hayashi, A. P. Côté, H. Furukawa, M. O'Keeffe, O. M. Yaghi, *Nat. Mater.* **2007**, *6*, 501 – 506.
[35] S. R. Venna, M. A. Carreon, *J. Am. Chem. Soc.* **2010**, *132*, 76 – 78.
[36] H. Bux, A. Feldhoff, J. Cravillon, M. Wiebcke, Y.-S. Li, J. Caro, *Chem. Mater.* **2011**, *23*, 2262 – 2269.
[37] A. Huang, H. Bux, F. Steinbach, J. Caro, *Angew. Chem. Int. Ed.* **2010**, *49*, 4958 – 4961; *Angew. Chem.* **2010**, *122*, 5078 – 5081.
[38] G. Lu, J. T. Hupp, *J. Am. Chem. Soc.* **2010**, *132*, 7832 – 7833.
[39] H. Jiang, B. Liu, T. Akita, M. Haruta, H. Sakurai, Q. Xu, *J. Am. Chem. Soc.* **2009**, *131*, 11302 – 11303.
[40] C. M. Miralda, E. E. Macias, M. Zhu, P. Ratnasamy, M. A. Carreon, *ACS Catal.* **2012**, *2*, 180 – 183.
[41] Y. Hu, H. Kazemian, S. Rohani, Y. Huang, Y. Song, *Chem. Commun.* **2011**, *47*, 12694 – 12696.
[42] C.-Y. Sun, C. Qin, X.-L. Wang, G.-S. Yang, K.-Z. Shao, Y.-Q. Lan, Z.-M. Su, P. Huang, C.-G. Wang, E.-B. Wang, *Dalton Trans.* **2012**, *41*, 6906 – 6909.
[43] S. A. Moggach, T. D. Bennett, A. K. Cheetham, *Angew. Chem. Int. Ed.* **2009**, *48*, 7087 – 7089; *Angew. Chem.* **2009**, *121*, 7221 – 7223.
[44] G. Kaur, R. K. Rai, D. Tyagi, X. Yao, P.-Z. Li, X. Yang, Y. Zhao, Q. Xu, S. K. Singh, *J. Mater. Chem. A* **2016**, *4*, 14932 – 14938.
[45] H. T. Kwon, H.-K. Jeong, A. S. Lee, H. S. An, J. S. Lee, *J. Am. Chem. Soc.* **2015**, *137*, 12304 – 12311.
[46] C. Wang, F. Yang, L. Sheng, J. Yu, K. Yao, L. Zhang, Y. Pan, *Chem. Commun.* **2016**, *52*, 12578 – 12581.
[47] H. Yang, X.-W. He, F. Wang, Y. Kang, J. Zhang, *J. Mater. Chem.* **2012**, *22*, 21849 – 21851.
[48] J. P. Patterson, P. Abellan, M. S. Denny, C. Park, N. D. Browning, S. M. Cohen, J. E. Evans, N. C. Gianneschi, *J. Am. Chem. Soc.* **2015**, *137*, 7322 – 7328.
[49] Y. Pan, D. Heryadi, F. Zhou, L. Zhao, G. Lestari, H. Su, Z. Lai, *CrystEngComm* **2011**, *13*, 6937 – 6940.
[50] I. H. Lim, W. Schrader, F. Schüth, *Chem. Mater.* **2015**, *27*, 3088 – 3095.
[51] B. Pattengale, S. Yang, J. Ludwig, Z. Huang, X. Zhang, J. Huang, *J. Am. Chem. Soc.* **2016**, *138*, 8072 – 8075.
[52] P. Y. Moh, P. Cubillas, M. W. Anderson, M. P. Attfield, *J. Am. Chem. Soc.* **2011**, *133*, 13304 – 13307.
[53] M. Tu, S. Wannapaiboon, R. A. Fischer, *Inorg. Chem. Front.* **2014**, *1*, 442 – 463.
[54] S. Saha, S. Springer, M. E. Schweinefuß, D. Pontoni, M. Wiebcke, K. Huber, *Cryst. Growth Des.* **2016**, *16*, 2002 – 2010.
[55] Y. Liu, N. Wang, J. H. Pan, F. Steinbach, J. Caro, *J. Am. Chem. Soc.* **2014**, *136*, 14353 – 14356.
[56] E. L. Bustamante, J. L. Fernández, J. M. Zamaro, *J. Colloid Interface Sci.* **2014**, *424*, 37 – 43.
[57] X. Xu, Y. Sun, Q. Zhang, S. Wang, L. Zhang, Z. Wu, G. Lu, *ChemistrySelect* **2016**, *1*, 1763 – 1767.

[58] J. Yao, R. Chen, K. Wang, H. Wang, *Microporous Mesoporous Mater.* **2013**, *165*, 200 – 204.
[59] M. He, J. Yao, Q. Liu, K. Wang, F. Chen, H. Wang, *Microporous Mesoporous Mater.* **2014**, *184*, 55 – 60.
[60] K. Zhou, B. Mousavi, Z. Luo, S. Phatanasri, S. Chaemchuen, F. Verpoort, *J. Mater. Chem. A* **2017**, *5*, 952 – 957.
[61] P. Krokidas, M. Castier, S. Moncho, D. N. Sredojevic, E. N. Brothers, H. T. Kwon, H.-K. Jeong, J. S. Lee, I. G. Economou, *J. Phys. Chem. C* **2016**, *120*, 8116 – 8124.
[62] K. H. Schmidt, A. Mueller, *Inorg. Chem.* **1975**, *14*, 2183 – 2187.

Manuscript received: May 11, 2017
Accepted manuscript online: July 1, 2017
Version of record online: July 24, 2017

